JOURNAL OF MATERIALS SCIENCE 26 (1991) 2743–2749

The role of the SnO_2 interphase in an alumina/glass composite: a fractographic study

M. H. SIADATI, K. K. CHAWLA
Department of Materials and Metallurgical Engineering, New Mexico Institute of Mining and Technology, Socorro, NM 87801, USA

M. FERBER
High Temperature Materials Laboratory, Oak Ridge National Laboratories, Oak Ridge, TN 37831, USA

The role of tin dioxide (SnO_2) interphase for the alumina/glass composite system was investigated using fractography. Alumina (Al_2O_3) and glass form a strong chemical bond which is undesirable for toughness in a ceramic matrix composite. SnO_2 interphase was incorporated to prevent this strong bond between alumina and glass. SnO_2 was deposited on Al_2O_3 substrates via chemical vapour deposition and bonded with glass. The role of the interphase was then studied by characterizing the fracture surfaces of the bend test and special composite disc samples loaded in diametral compression. Bend tests results showed that the SnO_2 interphase and/or the SnO_2/Al_2O_3 interface acted as a plane of weakness. Secondary cracking at 90° to the major crack direction was observed along this plane of weakness, which appears to be in accord with the Cook and Gordon model. Crack deflection and secondary cracking were also observed in the SnO_2 region of the compression samples. These results indicate the suitability of SnO_2 interphase for the alumina/glass composite system.

1. Introduction

The high thermal stability and elastic modulus of ceramic materials coupled with their low density and corrosion resistance make them very attractive for high-temperature applications [1]. Ceramic materials, however, lack toughness. Currently, a considerable amount of research is being directed at improving their toughness. One of the major efforts in this regard has been devoted to fibre-reinforced composites, particularly those reinforced with carbon, SiC, and alumina fibres [2]. Carbon fibre-reinforced glass matrix composites [3] have shown a wide range of attributes which include high strength, high stiffness, excellent toughness, and low density. SiC fibre-reinforced glasses and glass-ceramics have also shown a good combination of strength and toughness [2]. The toughness improvement in both carbon [4] and SiC [2, 5] fibre-reinforced composites has been attributed to the weak bonding between the fibre and matrix leading to fibre pullout before fracture. Studies of thermal stability of these composites have shown oxidation of carbon fibres in air [6] and gradual strength degradation of the SiC fibre in almost any environment when exposed to temperature as high as 1200 °C or more [7]. Thus, it would appear that the application of ceramic composites reinforced with either carbon or SiC fibres is limited as far as high-temperature use is concerned.

Alumina fibre-reinforced glass was shown to be unaffected by exposure to temperatures up to 1000 °C; however, the overall levels of toughness and strength obtained were less than those achieved through the use of carbon fibre-reinforcement [2]. The low toughness and strength mainly result from the dissolution of alumina fibres into the glass matrix producing a very strong chemical bonding between the two components [8–10]. An approach to overcome this problem involves interface engineering. The basic idea is to incorporate an interphase layer between fibre and matrix that would act as a diffusion barrier between the two components and limit the interface bond strength so that debonding can occur during passage of a crack. Bender *et al.* [11] showed the effect of fibre coating on the toughness improvement of silicon carbide fibre-reinforced zirconia composite. The thin boron nitride (BN) coating used in their investigation (1–2 μm thick) prevented any dissolution of fibre into the matrix. Other investigators employed BN coating on silicon carbide fibre in various matrices [12, 13] and obtained lower interfacial shear stress which resulted in a more extensive fibre pullout during the composite fracture. For alumina/glass composite, Maheshwari *et al.* [10] studied the effect of SnO_2 coating. The Al_2O_3–SnO_2 phase diagram predicts no mutual solid solubility at temperatures as high as

0022–2461/91 $03.00 + .12

1620 °C [14]. Maheshwari *et al.* obtained elemental concentrations at intervals of 2 μm across the two interfaces. They investigated diffusion of Sn, Si, and Al across the Al_2O_3/SnO_2 and SnO_2/glass interfaces using electron microprobe. Diffusion profiles for Sn, Si and Al showed, as expected, little evidence of diffusion across the alumina/SnO_2 interface at high temperatures. However, small amounts of Sn, Si, and Al diffused across the SnO_2/glass interface. Therefore, they concluded that the lack of solid solubility of SnO_2 in Al_2O_3 and very low solubility in glass at high temperatures coupled with its refractoriness make SnO_2 an ideal candidate for producing an interphase for the alumina/glass composite system. They also obtained some preliminary results from indentation cracking technique showing the ability of SnO_2 to cause crack deflection at the Al_2O_3/SnO_2 interface. A suitable interphase must provide a weak enough interface/ interphase to allow crack deflection and fibre pullout. If the Al_2O_3/SnO_2 interface and/or the SnO_2 interphase itself are weak enough, then either one of them or both can provide planes of weakness in front of an oncoming crack to cause crack deflection and/or secondary cracking [15]. The objective of this fractographic study was to examine this phenomenon in detail.

2. Materials and experimental procedure

The materials used for this experiment were polycrystalline α-alumina (99.5%) and a borosilicate type glass (N51A). The nominal composition of the glass is given in Table I. Stannic chloride ($SnCl_4$) was used to chemically vapour deposit (CVD) tin dioxide (SnO_2) on to alumina substrates. Table II gives some physical and mechanical properties of tin dioxide along with those of alumina and glass.

TABLE I Nominal composition of N51A glass [17]

	wt %		wt %
SiO_2	72	Si	33.6
B_2O_3	12	B	3.8
Al_2O_3	7	Al	3.7
CaO	1	Ca	0.7
Na_2O	6	Na	4.5
K_2O	2	K	1.7
BaO	< 0.1	Ba	trace
		O_2	balance.

TABLE II Important mechanical and physical properties of alumina, tin dioxide and glass

	Alumina	SnO_2	Glass
E (GPa)	360–400 [18]	233 [19]	72 [17]
VHN (GPa)	1.73 [20]	1.13 [20]	0.63 [20]
K_{Ic} (MPa $m^{1/2}$)	2.6 ± 0.1 [9]	?	0.7–0.8 [9]
ρ (g cm^{-3})	3.9–4.0 [18]	6.95 [21]	2.3 [17]
α (10^{-6} $°C^{-1}$)	7.4 [22]	3.77 [19]	7 [17]
Melting point (°C)	2015–2050 [23]	1630 [21]	–
Annealing point (°C)	–	–	570 [17]
Softening point (°C)	–	–	785 [17]

For bend tests, alumina substrates were surface finished to 600 grit paper. SnO_2 interphase was obtained by CVD at 750 °C for 20 min. Oxygen was used as a carrier gas for both water vapour (0.5 l min^{-1}) and $SnCl_4$ (1 l min^{-1}) in separate reactors and then fed into the ceramic tube reactor where the deposition of SnO_2 took place. By altering the oxygen flow, one could optimize the humidity level of the system to obtain reproducible coatings. SnO_2-coated and uncoated alumina substrates were bonded to glass at 900 °C for 1 h. Fig. 1 shows schematically a coated composite sample. A straight notch was introduced at the centre of the component on the tension side to control the crack initiation. Straight notches were made with a diamond wafer blade to a depth of about 1 mm. Bend tests were conducted in an Instron machine using a crosshead speed of 0.005 cm min^{-1}.

The same procedure was followed to coat Al_2O_3 ring samples and subsequently bond them with the glass, Fig. 2. The resulting composite discs were

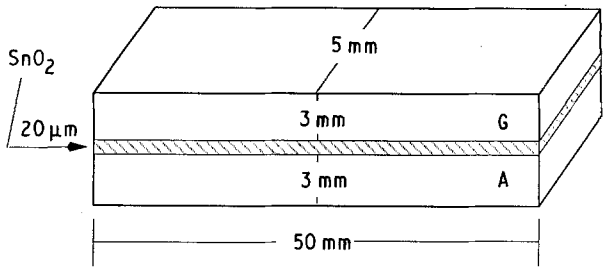

Figure 1 Schematic drawing of a coated composite sample showing the various components. A and G indicate alumina and glass, respectively.

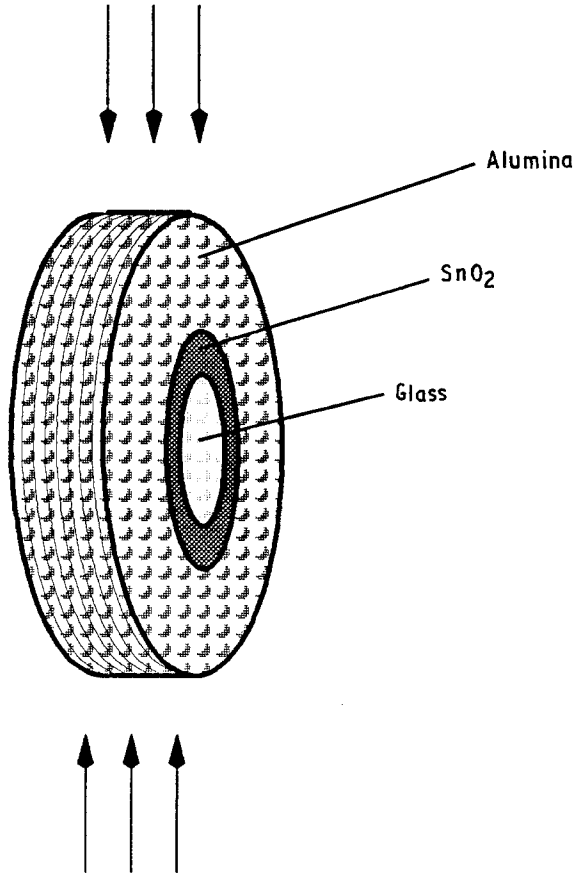

Figure 2 Schematic drawing of a composite disc sample.

loaded in diametral compression [16]. This geometry provides a simple method for obtaining a tensile stress normal to the interface/interphase. The compression tests were interrupted periodically and the composite discs were observed with a metallograph and SEM for any possible cracking or debonding at the interface/interphase. Fracture surfaces were examined by SEM.

3. Results and discussion

3.1. Bend test

Some features of the fracture surfaces of several notched alumina/glass bars broken in bend tests are described below.

Figs 3 and 4 show the relatively flat fracture surfaces of uncoated and coated samples, respectively. Figs 3b and 4b show the interface/interphase regions of Figs 3a and 4a at higher magnification (arrows indicate crack propagation direction). The uncoated sample (Fig. 3) showed a very intact and solid interface. The coated sample, however, showed secondary cracking, e.g. in the region marked by a rectangle in Fig. 4b. At still higher magnification, secondary cracks along the Al_2O_3/SnO_2 interface (Fig. 5a) and in the SnO_2 interphase (Figs 5b and 6) were clearly observable.

Careful observation and comparison of Figs 5 and 6 reveal that the features, in the plane of the picture (the primary crack), on the fracture surface of Fig. 5, are all discontinuous across the secondary crack. That discontinuity indicates that the secondary crack passed through the plane of the micrograph before the primary crack arrived. In Fig. 6, the fracture surface features are continuous. The occurrence of secondary cracks with discontinuous fracture surface features may be explained by considering the state of stress at the crack tip as analysed by Cook and Gordon [15]. Their analysis gives the stress distribution near the crack tip for various applied stress systems, e.g. uniaxial tension or wedge opening. It turns out that the stress distribution near the crack tip is about the same for different stress systems. Along the main crack direction (i.e. x-axis) σ_y is initially very high, but it falls sharply, Fig. 7. However, σ_x increases from zero at the crack tip and at a small distance (roughly equal to one crack tip radius as per Cook and Gordon model) reaches a maximum, the value of which is about one-fifth of the maximum value of σ_y (i.e. $\sigma_{x\,max} \simeq \frac{1}{5}\sigma_{y\,max}$). As one moves along the x-axis away from the crack tip and past the maximum value of σ_x, the two stresses σ_y and σ_x soon become roughly equal to each other and fall off together roughly as the inverse square root of

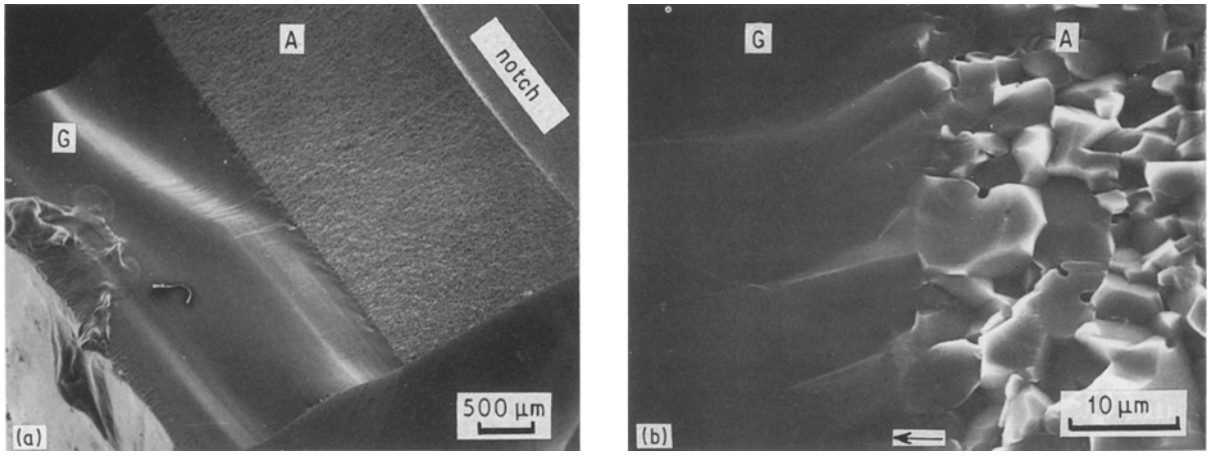

Figure 3 (a) Fracture surface of an uncoated Al_2O_3/glass composite at low magnification. (b) As (a); the arrow indicates the crack propagation direction. Note the integrity of the alumina/glass interface.

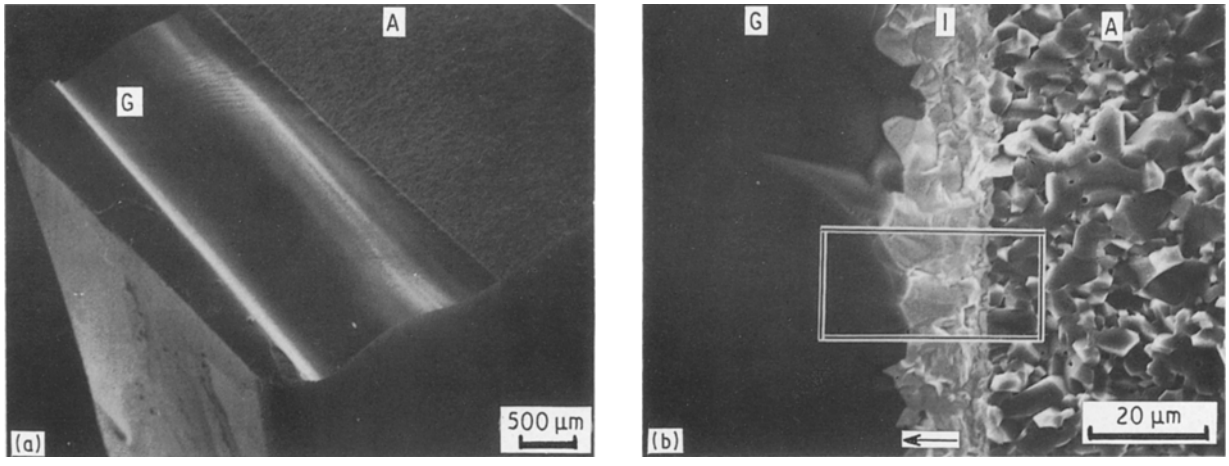

Figure 4 (a) Fracture surface of a coated Al_2O_3/glass composite at low magnification. (b) As (a); the area in the rectangle contains secondary cracks. The arrow indicates the crack propagation direction.

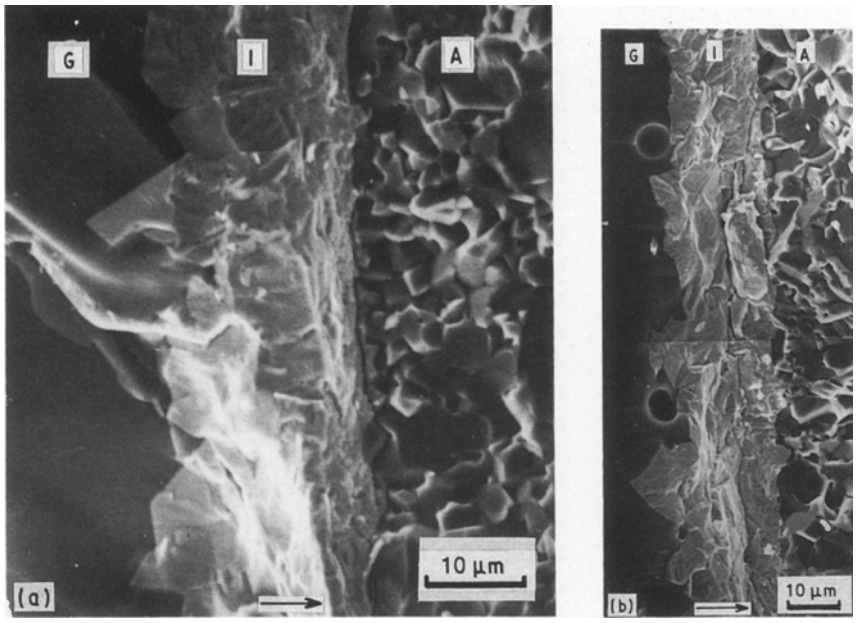

Figure 5 (a) Secondary crack at the SnO_2/Al_2O_3 interface. (b) Secondary crack in the SnO_2 interphase. The fracture surface features are not continuous across the crack.

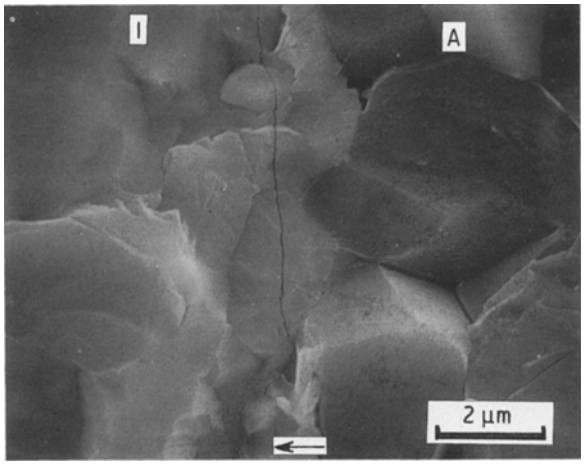

Figure 6 Secondary crack in the SnO_2 interphase near the SnO_2/Al_2O_3 interface. The fracture surface features are continuous across the crack.

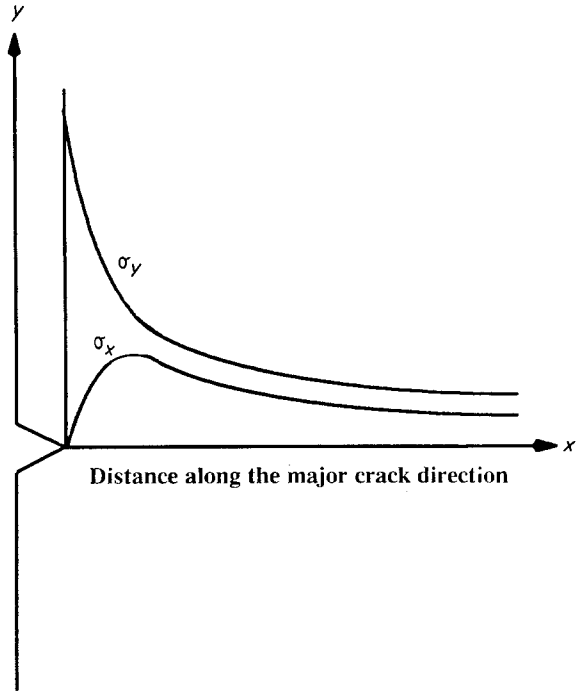

Figure 7 State of stress at a crack tip. Along the x-axis, σ_y, although initially high, falls sharply. However, σ_x increases from zero at the crack tip and, at a distance roughly equal to one crack tip radius, reaches a maximum value which is about one-fifth of the maximum value of σ_y [15].

the distance from the crack tip. Fig. 8 shows a schematic drawing of a three-point bend laminate composite sample after the application of load. Analogous to the stress analysis of Cook and Gordon [15], a triaxial state of stress prevails at the crack tip under load. σ_y and σ_x are indicated in Fig. 8, σ_z if present (plane strain) will act perpendicular to the plane of the figure. Also shown in Fig. 8 are the secondary cracks as observed in the present work. Fig. 9 shows the long transverse side of a four-point bend sample broken at 500 °C. Note the debonding along the Al_2O_3/SnO_2 interface caused by formation of secondary cracking. It would appear that these secondary cracks at Al_2O_3/SnO_2 interface or in SnO_2 would have formed as per the mechanism suggested by Cook and Gordon. This mechanism indicates that if the interface is weak enough, it will crack open some distance ahead of the primary crack forming a secondary crack as shown in Fig. 10.

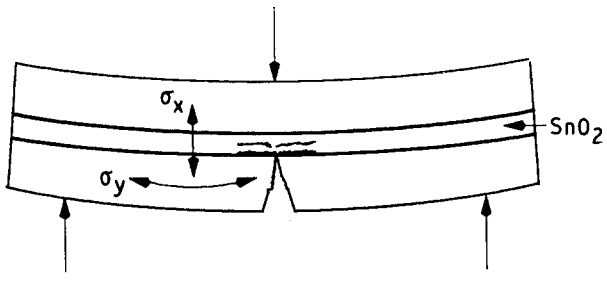

Figure 8 Bend test specimen after the application of load showing secondary cracking in the interphase layer.

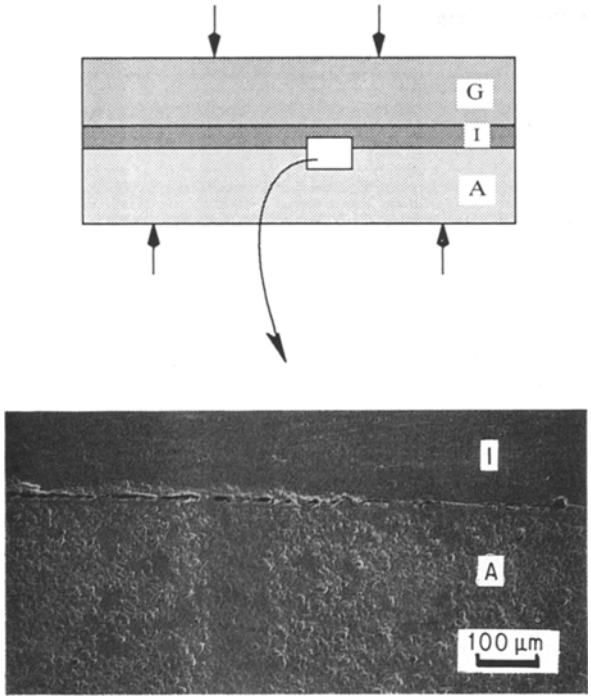

Figure 9 Long transverse view of a four-point bend test specimen after fracture at 500 °C. Note the debonding along the Al_2O_3/SnO_2 interface caused by formation of secondary cracking.

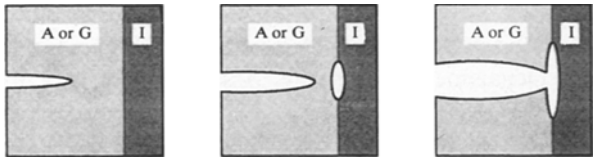

Figure 10 Fracture of the interface some distance ahead of the primary crack [15].

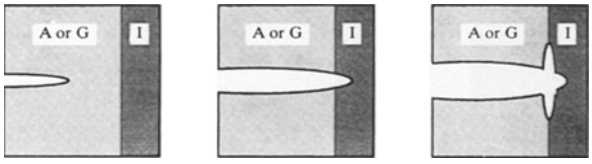

Figure 11 Penetration of the primary crack through the interface which may crack immediately behind the primary crack tip [15].

In cases where there exists a continuity of features on the primary fracture surface across the secondary crack (Fig. 6), Cook and Gordon considered the case of primary crack penetration through the interface which may crack open afterwards. According to this model which is schematically shown in Fig. 11, the interface opens up behind the primary crack tip to yield a cruciform-shaped crack. What is important to emphasize at this point is that this later secondary crack formation also represents an energy-consuming feature of the overall fracture process, and hence a contribution to toughness.

In both cases, the occurrence of secondary cracking or crack deflection provides an energy-dissipating mechanism in the alumina/glass composite system.

3.2. Compression test

The main reason for using this special test was to exploit the difference between the Poisson's ratios of alumina and glass (0.27 and 0.21, respectively). This difference was expected to cause debonding at the alumina/glass interface under compression. This debonding could occur if the transverse elastic stress generated due to the difference in Poisson's ratios was larger than the strength of the alumina/glass interface. Compression tests performed on uncoated samples revealed no debonding at the interface. The absence of debonding along the alumina/glass interface is a good indication that the elastic stress generated due to the difference in Poisson's ratios is smaller than the strength of the alumina/glass interface.

The coated disc sample broke into two halves just as the uncoated one did. Fig. 12 shows schematically a broken half of the coated sample. The fracture surface was observed in the SEM and, not unexpectedly, secondary cracks were observed at various locations within the SnO_2 interphase. Fig. 13 shows one such secondary crack. This crack may have initiated at the alumina/SnO_2 interface, then entered the SnO_2 interphase, extending almost parallel to the interface and

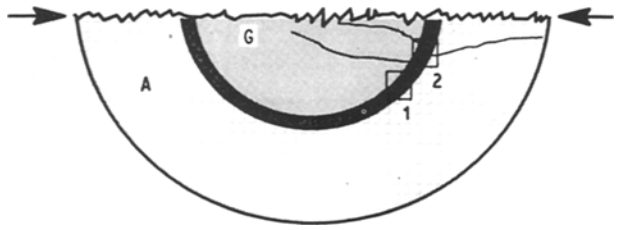

Figure 12 Schematic drawing of a composite disc sample broken under compression. The arrows indicate the compression direction.

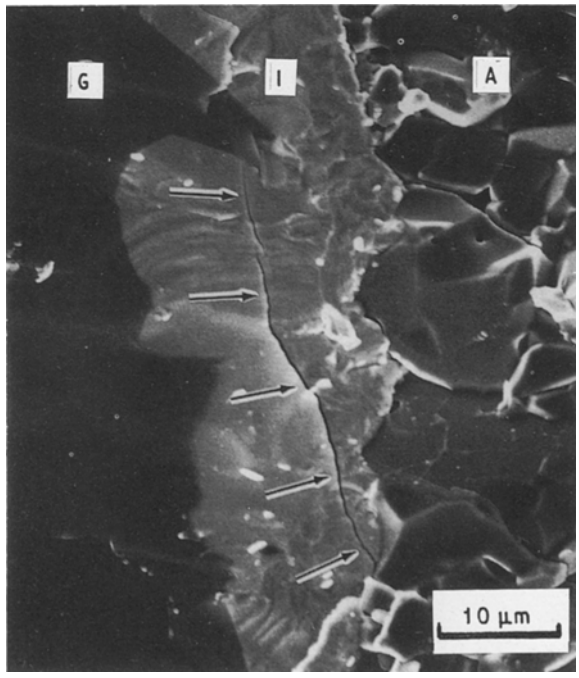

Figure 13 Fracture surface of a coated composite disc sample. Arrows show a secondary crack in the SnO_2 region. Note the surface features are continuous.

terminating there. On the face normal to the fracture surface, extensive cracking also occurred at various locations of the SnO_2 interphase. Fig. 14, high magnification view of rectangle 1 in Fig. 12, shows the cracking in the SnO_2 interphase very clearly. The phenomenon of crack deflection at the location marked by rectangle 2 is shown in Fig. 15. Three deflected cracks marked A, B, and C are shown at higher magnification in Fig. 15. The other end of each of the three is portrayed in the schematic drawing in Fig. 12; b and c end in glass and d in alumina. The crack pattern in this figure does have the proper general character of fracture as per the Cook and Gordon mechanism.

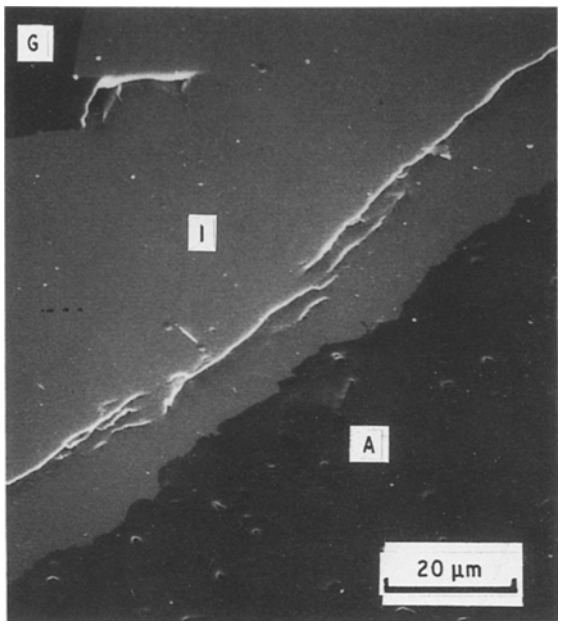

Figure 14 Magnified view of rectangle 1 marked in Fig. 12, illustrating cracking of SnO_2 at this location.

4. Conclusions

From this fractographic study on the role of SnO_2 in alumina/glass composites, we can draw the following conclusions.

1. Observation of secondary cracking at the Al_2O_3/SnO_2 interface and/or within the SnO_2 region on the fracture surfaces of the bend samples confirmed the weakness of both the Al_2O_3/SnO_2 interface and the SnO_2 interphase. This secondary cracking appears to be in accord with the Cook and Gordon model.

2. Crack deflection in the SnO_2 region of the disc-shaped composites, and the absence of such a phenomenon in the uncoated samples, also proved the eventual toughening capability of the SnO_2 interphase.

Acknowledgements

This work was supported by Sandia National Laboratories (contract 05-1773) and Office of Naval Research (contract N00014-89-J-1459). Helpful discussions with Dr E. K. Beauchamp are greatly appreciated. Research was also sponsored in part by the US Department of Energy, Assistant Secretary for Conservation and Renewable Energy, Office of Transportation Systems, as part of the High Temperature

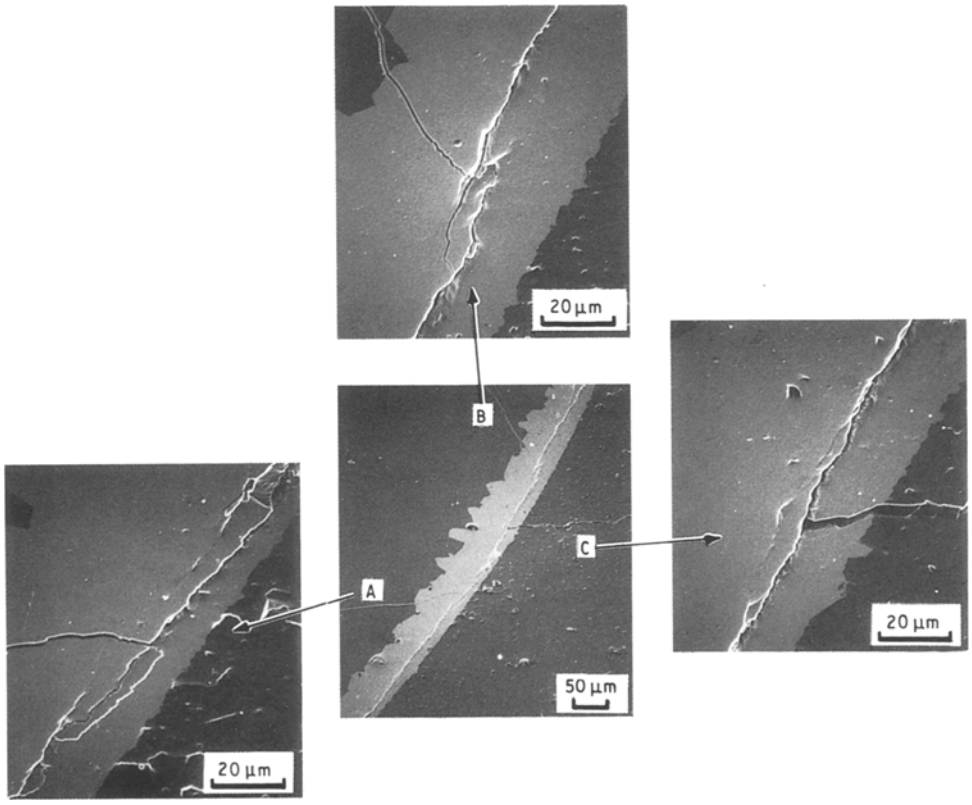

Figure 15 Magnified views of rectangle 2 marked in Fig. 12, showing extensive cracking of SnO_2 together with deflection of three cracks marked A, B, and C. The crack pattern in this figure has the proper general character of fracture as per the Cook and Gordon mechanism.

Materials Laboratory User Program, under contract DE-AC05-840R21400 with Martin Marietta Energy Systems, Inc.

References

1. K. K. CHAWLA, "Composite Materials: Science and Engineering" (Springer-Verlag, New York, 1987) p. 134.
2. K. M. PREWO, J. J. BRENNAN and G. K. LAYDEN, *Ceram. Bull.* **65** (1986) 305.
3. K. M. PREWO and J. F. BACON, "Glass Matrix Composites-I, Graphite Fibre Reinforced Glass", in "Proceedings of the Second International Conference on Composites", edited by B. R. Nòrton (TMS-AIME, New York, 1974) p. 64.
4. R. LEVITT, *J. Mater. Sci.* **8** (1974) 1847.
5. J. J. BRENNAN and K. M. PREWO, *ibid. J. Mater. Sci.* **17** (1982) 2371.
6. K. M. PREWO and J. A. BATT, *ibid.* **24** (1988) 523.
7. T. MAH, N. L. HECHT, D. E. McCULLUM, J. R. HOENIGMAN, H. M. KIM, A. P. KATZ and H. A. LIPSITT, *ibid.* **19** (1984) 1191.
8. J. L. KEDDIE and T. A. MICHALSKE, "Interface structure and Properties of Alumina/glass ceramic composite", Sandia Report SAND 87-1884, UC-25, January 1988.
9. T. A. MICHALSKE and J. HELLMANN, *J. Amer. Ceram. Soc.* **71** (1988) 725.
10. A. MAHESHWARI, K. K. CHAWLA and T. A. MICHALSKE, *Mater. Sci. Engng* **A107** (1989) 269.
11. B. BENDER, D. SHADWELL, C. BULIK, L. INCORVATI and D. LEWIS III, *Amer. Ceram. Soc. Bull.* **65** (1986) 363.
12. M. K. BRUN and R. N. SINGH, *Adv. Ceram. Mater.* **3** (1988) 506.
13. R. N. SINGH, *J. Amer. Ceram. Soc.* **72** (1989) 1764.
14. V. J. BARCZAK and R. H. INSLEY, *ibid.* **45** (1962) 144.
15. J. COOK and J. E. GORDON, *Proc. R. Soc. Lond.* **A282** (1964) 508.
16. A. RUDNICK, C. W. MARSHALL, W. H. DUCKWORTH and B. R. EMRICH, "Evaluation and Interpretation of Mechanical Properties of Brittle Materials", Battell Memorial Institute, Columbus, Ohio, Air Force Materials Laboratory Contract AF33(615)-2335, Tech. Report. AFML-TR-67-316, DCIC68-3 (1967) pp. 191.
17. Owens-Illinois Inc, Personal communication (1987).
18. K. K. CHAWLA, "Composite Materials: Science and Engineering" (Springer-Verlag, New York, 1987) p. 77.
19. J. QUIRK and C. G. HARMAN, *J. Amer. Ceram. Soc.* **37** (1954) 24.
20. A. MAHESHWARI, MS thesis, New Mexico Institute of Mining and Technology, Socorro, NM (1988).
21. R. C. WEAST (ed.), "CRC Handbook of Chemistry and Physics", 67th Edn (CRC Press, Boca Raton, FL, 1986) p. B-140.
22. R. N. KLEINER, in "Handbook of Materials Science", edited by C. T. Lynch (CRC Press, Cleveland, OH, 1975) p. 335.
23. I. W. DONALD and P. W. McMILLAN, *J. Mater. Sci.* **11** (1976) 949.

Received 19 April
and accepted 2 August 1990